

Dynamic Modeling of Turbulent Shedding Effect on the 30-meter Primary Mirror of GSMT

Guanpeng Xu^{1a}, Mark Whorton^{2b}, Yong X. Tao^{3c}, Myung Cho^{4d}

^aTennessee State University, ^bNASA, ^cFlorida International University, ^dAURA NIO

ABSTRACT

This paper presents a Navier-Stokes based numerical methodology for three-dimensional unsteady viscous flow over a general mirror configuration. In this approach, the Reynolds averaged Navier-Stokes equations in finite volume form are solved unsteadily using Roe's scheme on body fitted H-H type grid. A two-equation turbulence model, the k- ϵ turbulence model, was implemented. This method is three or five order accurate in space and first order accurate in time. The physical space modeled is a 120m \times 120m \times 120m region enclosing the primary mirror at the center. The inflow turbulence from the enclosure openings is represented by turbulence kinetic energy at the inflow boundary. The wind buffeting effect was studied by directly calculating flow field response to buffeting impinging wind. The unsteady pressure distribution on the mirror is extracted and analyzed for the amplitudes and frequencies of dynamic wind loading. The computational results are visualized to highlight the flow pattern, particularly on the mirror upper surface. Results are presented for a 30-meter aperture GSMT primary mirror. A 1:833 model of the GSMT primary mirror was tested in a water tunnel, in which the velocity distribution was measured using PIV technique. The preliminary experimental observation serves as qualitative validation of the simulation capability.

Keywords: wind buffeting, Navier-Stokes equations, Unsteady, wind loading, Roe's scheme, k- ϵ turbulence model, primary mirror, GSMT, water tunnel, PIV

1. INTRODUCTION

Ground-based telescopes with sensitivity comparable to next generation space-based and radio facilities are essential to future astrophysical research. A 30-meter aperture Giant Segment Mirror Telescope (GSMT) was recommended by the Astronomy and Astrophysics Survey Committee (AASC). The New Initiatives Office (NIO) of Association of Universities for Research in Astronomy (AURA), Inc. was established to work on the design and future construction of the 30-meter aperture GSMT. The importance of the 30-meter aperture GSMT and the technique issues that need to be solved in the design phase have been documented in *The GSMT Book: Enabling a Giant Segmented Mirror Telescope for the Astronomical Community*, which is authored by more than 50 contributors coordinated by the NIO¹.

For the next generation of giant ground-based telescopes, preliminary studies have shown that wind loading is the most significant disturbance to the telescope structure. Figure 1 shows the point design GSMT dome structure. Three openings are shown on the dome in Figure 1. The front opening is for the primary mirror facing the stars of interest, so it has to follow the direction to which the telescope points. Two side-openings allow natural wind to blow across the primary telescope mirror. The ventilating wind from two side-openings causes two effects on the image quality of the GSMT. The first effect, which is beneficial to image quality, is the removal of uneven temperature gradients, or hot spots, in the telescope enclosure. The second effect, which is harmful to image quality, is the possible structural

¹ xu@coe.tsuniv.edu; phone 1 615 963-7280; fax 1 615 963-7027; Center of Excellence, Tennessee State University, 330 10th Avenue North, Nashville, TN 37203-3401

² mark.whorton@msfc.nasa.gov; phone 256-544-1435; NASA Marshall Space Flight Center, TD55/Control Systems, Huntsville, AL, USA 35812 (NASA Administrator's Fellow at The Tennessee State University, Center of Excellence in Information Systems, Nashville, TN)

³ taoy@fiu.edu; phone 1 305 348-3015; fax 1 305 348-1932; Department of Mechanical Engineering, Florida International University, Miami, FL 33174.

⁴ mcho@gemini.edu; phone 1 520 318-8544; fax 1 520 318-8590; AURA New Initiatives Office, 950 N. Cherry Ave., Tucson, AZ, USA 85719.

vibration due to dynamic wind loading, especially when the frequency of the dynamic wind loading is close to the structural resonant frequencies, which can be as low as 2 Hz according to NIO point design. The amplitude and strength properties of the unsteady wind loading on the primary mirror surface at every mirror segment under different ambient wind conditions are essential to designing a cost-effective telescope without losing image quality.

Using computational fluid dynamics (CFD) methodology, a wide variety of wind conditions and enclosure/telescope configurations can be studied. Using an incompressible, steady state three-dimensional CFD package, De Young studied a circular mirror shape and a cylindrical telescope configuration². However, the steady-state feature of the solver limited its application for dynamic wind modeling. Extensive unsteady measurements were conducted for the wind buffeting effect on the Gemini 8m telescope³.

The present work is motivated by the need for a first-principles based analysis that will faithfully model the complexities of the 3-D unsteady viscous flow over the telescope mirror, but remain economical enough for point design use. In the present work, the telescope mirror is modeled using 3-D Reynolds averaged Navier-Stokes (RaNS) equations. To simplify the grid generation and reduce the number of grid nodes, only the telescope primary mirror is studied. The physical domain modeled is a cubic space enclosing the primary mirror, and the physical domain extends to 60 meters upwind, downwind and to the other sides. The wind turbulence and buffeting from the enclosure openings is introduced at the inflow boundary.

The flow field surrounding the primary mirror is separated, incompressible, viscous and with heat transfer. Modeling the viscous region using methodologies for incompressible Navier-Stokes equations would omit the heat transfer effect and require a costly iterative method at every time step for unsteady calculation. For this reason, the present approach models the telescope mirror flow using compressible Navier-Stokes equations. At low Mach numbers, the compressible and incompressible analyses will yield identical results, as dictated by the physics of the problem. Thus, no errors are caused by assuming the flow to be compressible.

The present methodology has been previously applied to various fixed wing and rotary flight vehicles^{4,5}. The solving module of the present research code was first developed at Professor Lakshmi N. Sankar's group of Georgia Institute of Technology⁶.

In addition to the numerical studies, an experimental effort has been made to understand the primary mirror flow using a water tunnel and Particle Imaging Velocimetry (PIV) measurement upon a reduced telescope model. The water tunnel study was conducted at Florida International University (FIU). The preliminary results for water tunnel measurements are also documented in the present paper.

This paper is organized as follows. The mathematical formulation behind the Navier-Stokes and the k-ε turbulence model is first described. Procedures for wind turbulence and buffeting effects from ambient air and edges of enclosure openings are next documented. Then, numerical results are presented for the conceptual primary mirror designed by the AURA New Initiatives Office for the 30meter aperture GSMT. The numerical results and methodologies with the water tunnel PIV measurements are examined to establish the reliability and accuracy of present application. This paper is closed by concluding remarks on the point design from present CFD studies and future work.

2. NUMERICAL METHODOLOGY

2.1 Roe's Scheme

A three-dimensional, Navier-Stokes solver developed at Georgia Tech was modified for the present telescope studies. This analysis solves RaNS in finite volume form using Roe's scheme⁷. Details of the implementation of present methodology to a structural 3-D grid were documented in Reference 8. This methodology is up to 3rd or 5th order accurate in space, and 1st order accurate in time. The integral form RaNS for a finite volume V enclosed by surface S is:

$$\frac{d}{dt} \iiint_V q dV + \iint_S \vec{E}_l \cdot \vec{n} dS = \iint_S \vec{E}_v \cdot \vec{n} dS \quad (1)$$

Here, \vec{n} is the outward facing unit normal vector, and q is the commonly used flow vector consists density, ρ; three velocity components, u, v, w; and total energy per volume, e:

$$q = \begin{Bmatrix} \rho \\ \rho u \\ \rho v \\ \rho w \\ e \end{Bmatrix} \quad (2)$$

The quantities \vec{E}_I and \vec{E}_V are the inviscid and viscous fluxes. (ref. 8)

2.2 The k-ε Turbulence Model

Since the mirror flow is turbulence dominated separated flow, a two-equation turbulence model, k-ε turbulence model is used. In this model, the turbulent viscosity, μ_T , which is needed in the Navier-Stokes solver, is evaluated from two physical quantities, the turbulent kinetic energy k, and the dissipation rate ε, as

$$\mu_T = C_\mu \rho \frac{k^2}{\varepsilon} \quad (3)$$

The basic higher Reynolds number k-ε model integrates the following transport equations for k and ε⁹:

$$\rho \frac{Dk}{Dt} = \frac{\partial}{\partial X_i} \left(\frac{\mu_T}{\sigma_k} \right) \frac{\partial k}{\partial X_i} + P - \rho \varepsilon \quad (4)$$

and

$$\rho \frac{D\varepsilon}{Dt} = \frac{\partial}{\partial X_i} \left(\frac{\mu_T}{\sigma_\varepsilon} \right) \frac{\partial \varepsilon}{\partial X_i} + \frac{\varepsilon}{k} (C_1 P - C_2 \rho \varepsilon) \quad (5)$$

where P, the turbulent production, is given by

$$P = -\overline{\rho u_i u_j} \frac{\partial u_i}{\partial X_j} \quad (6)$$

Finally, the basic constants in the k-ε formulation are:

$$C_\mu = 0.09, C_1 = 1.43, C_2 = 1.92, \sigma_k = 1.0, \sigma_\varepsilon = 1.3$$

2.3 The Modeling of Wind Turbulence and Wind Buffeting Effects

The inflow wind turbulence due to opening edges on the telescope enclosure is modeled by assigning the turbulent kinetic energy, (TKE) k, according to the strength of turbulence at the upstream inflow boundary, as shown in Figure 2. The TKE is set to zero for laminar inflow, in present study, the non-dimensional TKE at inflow boundary is set as,

$$k = \langle u'^2 \rangle / \tilde{U}^2 \quad (7)$$

where the operator $\langle \rangle$ means temporal average, u' is the turbulent velocity and \tilde{U} is the same reference velocity as that was used for RaNS equations, which is the average wind speed. The value of $\langle u' \rangle$ at the inflow boundary can be obtained from unsteady measurements³.

The wind buffeting effect is studied by modeling unsteady buffeting wind directly. The vortex series shed from the enclosure opening edges and the gust wind from ambient air induce wind buffeting. The wind buffeting effect to dynamic wind loading is studied by introducing unsteady buffeting velocity U_b at the inflow boundary,

$$u_b(t) = U_b \sin(\omega t + \phi) \quad (8)$$

where ϕ is the initial phase angle, which is simply set to zero. $\omega = 2\pi f$, and U_b and f are the amplitude and frequency of the wind buffeting.

A reduced frequency, k_f , has to be defined to determine the numerical wind buffeting frequency from the real buffeting wind:

$$k_f = \frac{\omega D}{2U} \quad (9)$$

where D is the aperture of the primary mirror, which is 30 meter in the present study. U is the mean wind speed. The same reduced frequencies as in real cases are used in numerical modeling.

2.4 Water Tunnel Setup

A 1:833 model of the primary mirror was tested in the water tunnel at FIU. The test section of the water tunnel is 0.156m×0.131m with the Reynolds number based on the mirror diameter is about 3,000. A PIV system is used to measure the water velocity component in the plane that parallel to the water flow direction and normal or parallel to the mirror aperture. The vorticity field can be calculated from the velocity vector data obtained. The water tunnel has been used for several experimental studies of flow through melting packed beds¹⁰.

The model of the telescope features a circular edge, and the model upper surface is geometrically similar to the upper surface of the 30-meter GSMT primary mirror. The bottom of the model is simplified as a reversed circular cone. The results of model flow measurements serve as a preliminary validation of the numerical simulation. Figure 3 shows the photo of the mirror model standing in the test section of FIU water tunnel. The water velocity components on a two-dimensional plane, with seeding particles illuminated by pulse laser, are calculated by dividing the distances particles in water traveled by the time that is an ultra-short duration between laser pulse.

3. RESULTS AND DISCUSSION

Calculations and water tunnel experiment have been done for the 30-meter aperture GSMT primary mirror at several wind speeds and impinging angles. For numerical studies, the H-H type grid was generated using EagleView software developed at the Engineering Research Center (ERC) of Mississippi State University. Figure 4 shows the local and overall body fitted H-H grid around the primary mirror.

3.1 Validation of the Solving Module for the RaNS Equations

A cylinder is solved using the present methodology to validate the capability of modeling separated flow. An O-H type grid was used. Each section of the cylinder is a unit circle. Figure 5a shows one section of the O-H grid for cylinder. Figure 5b shows the traces of the fluid particles. These traces were generated by releasing fluid particles from grid nodes on a section of grid line. For steady flow, these traces are identical with streamlines. Visualization using fluid particle traces is the primary flow visualization method in present study.

Figure 5b shows a symmetric flow around the unit circle because the numerical methodology and the geometry all are symmetric. The vortex shedding after the circle was not observed from the numerical results.

The present methodology solves the compressible Navier-Stokes equations. However, wind flow at the telescope is incompressible. For typical wind speeds, such as 3 m/s, 8 m/s and 15 m/s, the Mach number is in the order of 0.01 to 0.05. The numerical convergence of the present methodology becomes harder when the Mach number is less than 0.1. On the other hand, flow physics dictates that the compressible and incompressible analyses will yield identical results for Mach number less than 0.3. Figure 6 shows the pressure coefficient distribution along the unit circle for Mach number 0.3 and Mach number 0.1. The Reynolds number was set as 2.44 million for both Mach numbers. The results are identical for attached flow region. The difference of the pressure coefficients after separation for Mach number 0.3 and 0.1 was because separation occurred at different places.

The primary mirror configuration is modeled as a thin mirror shape with sharp edge. The separation always occurs at the sharp edge of the telescope mirror. Throughout this present study, the numerical Mach number is set as 0.3. However, the effects of increasing Mach number in incompressible Mach number region (0 ~ 0.3) need further studies.

3.2 Results for the Primary Mirror with Circular Edge

As shown in Figure 4, a circular edge primary mirror was first studied using H-H grid. In addition to the flow field visualization using the traces of fluid particles, the unsteady wind loading was quantified in the form of dynamic wind loading vs. time at the relative positions shown in Figure 7 below. These points are numbered first from left to right, then

from centerline to top, as indicated in Figure 7. In each direction the spacing of points in the diagram is 5 meter and the center of the mirror is half way between grid points. The dynamic wind loading is defined as the pressure difference between upper and lower mirror surface at the points.

Figure 8 shows the flow field visualization for the round mirror configuration under 8 m/s impinging wind. The impinging angle is 0°, or wind blows in the mirror aperture plane. The Reynolds number is 13.7 million. From the top view for the mirror upper surface, Figure 8a, the calculated upper flow is symmetric and massively separated. As shown in the side view, Figure 8b, the separated flow is confined to a thin region next to the mirror surface, except for a gust that abruptly separates from mirror surface and shoots up at about 1.5 meter upstream of the mirror center.

The abrupt separation at 1.5 meter upwind the mirror center is due to the large size of the two main symmetric vortexes that follow the mirror leading edge. The abrupt separation is the joint effect of the combination of the two vortexes and the ambient mean flow above them.

Figure 9 shows the non-dimensional pressure contour on the upper and lower surface for the same impinging angle. As shown in figure 9a, the wind pressure variation pattern on the upper mirror shows a good agreement with the measured wind pressure pattern described in CHO.³ The conversion factor to the dimensional pressure in (N/m²) is $(\rho a^2)(M_{real}/M_{nominal})^2 \approx 695$ for 8 m/s wind, where ρ is air density, and a is the speed of sound. Therefore, the difference between the maximum and the minimum pressure in Figure 9 is about 50 N/m².

Figure 10 shows the flow pattern for the GSMT mirror in 8m/s wind under 35° degree impinging angle from above. Perfect flushing was observed on the mirror upper surface, as shown in Figure 10c. Complete separation was found under the primary mirror as shown in Figure 10a and 10b. Fluid particles for traces were released from the leading edge of the mirror for 10a, and from the trailing edge of the mirror for 10b, in which the fluid particles return back to places near the leading edge.

3.3 Effect of Serrated Edge due to the Hexagon Shape of Telescope Segments

Figure 11 shows the flow field visualization for the 30-meter GSMT mirror with a serrated edge. The serrated edge is due to the hexagon shape of mirror segment configuration. It is difficult to generate one set of structured body-fitted grid around this configuration. Modification, as highlighted in the circle in Figure 11b, has been made to eliminate singular grid nodes. Other ways to map the serrated edge can be either use unstructured grid or use multi-zone structured grid.

Comparison between Figure 11a and Figure 8a shows that the vortex structure for mirror with serrated edge is similar with that of round mirror at the upstream half. The main difference consists a) the strong turbulence shedding from the side saw-like edge, as shown in the ellipsoid in Figure 11a, and b) the absence of the abrupt separation as shown in Figure 8b. The reason for b) is that the serrated edge cuts big vortex into smaller vortexes, enhanced the mixing of air above the mirror.

The dynamic responses at the 16 points shown in Figure 7 were recorded in the form of pressure difference as a function of time. Figures 12a and 12b show the dynamic loading on point No. 1 and point No. 3 for the mirror with round and serrated edge. The dynamic oscillation is greatly reduced, especially for faster harmonics, for the mirror with serrated edge.

3.4 Wind Buffeting Effect

The effect of 0.5Hz, 2 m/s wind buffeting for 8 m/s mean wind was studied using direct calculation for the round edge mirror. Figure 13 shows the dynamic wind loading at point No. 1 and point No. 3 with wind buffeting effect. Little difference can be found between Figure 13 and Figure 12a for amplitude and frequency of the unsteady wind loading at these two points. This might be because the inflow boundary is too far from the mirror (105 m) and coarse grid is used at far field boundary. The effect of buffeting and turbulence at that far field is smoothed out by the coarse grid at far field and the dissipation on the long way to the mirror. So the effect of vortexes shed from the mirror leading edge dominates the dynamic wind loading at point No. 1 and point No. 3. More cases with different settings need to be studied for the effect wind buffeting.

3.5 Water Tunnel Measurements

Figure 14 and Figure 15 shows the typical velocity vectors and vorticity contours for water flow over the model mirror. The Reynolds number for this case is about 3,000. Arrows indicate velocity vectors, and color contour lines represent vorticity values.

Although this is a relatively low speed case, the results clearly show a flow disturbance caused by the leading edge of the mirror model. The dissipation of the leading edge vortices may cause the fluctuation of pressure on the mirror surface.

Differences between water tunnel measurement and CFD can be found by comparing Figure 14 with Figure 8b. From CFD results, the turbulence from the mirror leading edge is limited in a thin region on the mirror upper surface, as shown in Figure 8b. However, the water tunnel measurements (Figure 14) show the leading edge vorticity goes up, leaving the mirror surface. This difference may be caused by the significant difference in Reynolds numbers modeled.

Figure 15 shows the top view of the vorticity distribution on the horizontal plane about 2 mm above the edge of the mirror for flow over the mirror model. High vorticity near the leading edge is observed. However, comparing with symmetric separation found in CFD results, Figure 8a, the water tunnel measurement somehow shows asymmetric vortex shedding along the center plane. This may be caused by a slight non-uniformity in the main flow due to the influence of tunnel walls.

4. CONCLUDING REMARKS

The methodology for modeling the dynamic wind loading on the 30 meter GSMT primary mirror configuration has been established. The primary mirrors with round and serrated edges were studied. Procedures for studying wind buffeting and inflow wind turbulence effects have been established. The primary mirror flow was also experimentally studied in a water tunnel using reduced mirror model. The following conclusions may be drawn from the results presented in this paper:

- a) If the wind blows the mirror from side, (0° impinging angle), serrated edge cuts the larger vortices shed from the mirror leading edge into smaller ones, resulting in better mixing of airflow on the mirror upper surface, which means better image quality and lower amplitude of dynamic wind loading.
- b) If the wind can be directed so that it blows to the mirror surface at a positive angle, perfect flushing can be achieved on top of the primary mirror. The massive separation under the mirror will not be a problem, since there will be a very complex structure for support and control of each mirror segment. Similar to the effect of a serrated edge, the complex structure under the mirror will mince the big vortex shed under the mirror into smaller vortices such that the amplitude of dynamic wind loading can be reduced.
- c) The inflow wind turbulence and wind buffeting effects should be implemented at a close position to the primary mirror. In the cases studied, it seems the turbulence shed from the mirror leading edge dominates the flow around the mirror.

Further study is needed to investigate more cases where the measured wind buffeting and wind turbulence and finer grid are used to achieve a better understanding of the effect of turbulence shed from the enclosure opening and the mirror leading edge. Better understanding of scaling the water tunnel measurements under lower Reynolds number is needed to apply the water tunnel measurements to the design use of the future GSMT.

ACKNOWLEDGEMENTS

The authors would like to thank George Angeli and Larry Stepp of the NIO for their valuable suggestions.

This work was partially supported by the New Initiatives Office. The New Initiatives Office is a partnership between two divisions of the Association of Universities for Research in Astronomy (AURA), Inc.: the National Optical Astronomy Observatory (NOAO) and the Gemini Observatory. NOAO is operated by AURA under cooperative agreement with the National Science Foundation (NSF). The Gemini Observatory is operated by AURA under a cooperative agreement with the NSF on behalf of the Gemini partnership: the National Science Foundation (United States), the Particle Physics and Astronomy Research Council (United Kingdom), the National Research Council (Canada), CONICYT (Chile), the Australian Research Council (Australia), CNPq (Brazil) and CONICE (Argentina).

This work was also partially supported by NSF Grant HRD 6706268.

REFERENCES

1. <http://www.aura-nio.noao.edu/book/index.html>, "Enabling a Giant Segmented Mirror Telescope for the Astronomical Community", AURA New Initiatives Office.
2. De Young, D. S., "Numerical Simulations of Airflow in Telescope Enclosures," *The Astronomical Journal*, Volume 112, Number 6, pp 2896-2908, December, 1996.
3. M. K. Cho, L. M. Stepp, G. Z. Angeli, D. Smith, "Wind Loading of Large Telescopes," *Proceedings of SPIE 4837*, (2002). 4837-40.
4. Wake, B. E. and Sankar, L. N., "Solution of Navier-Stokes equations for the flow over a rotor blade", *Journal of the American Helicopter Society*, April 1989.
5. Hariharan, N., Sankar, L. N., "Higher Order Numerical Simulation of Rotor Flow Field," *AHS Forum and Technology Display*, Washington, DC., May 1994.
6. Guanpen Xu, "Computational Studies of Horizontal Axis Wind Turbines", *Doctoral Thesis*, School of Aerospace Engineering, Georgia Institute of Technology, Atlanta, GA 30332-0150.
7. Roe, P. L., "Approximate Riemann Solvers, Parameter Vectors, and Difference Schemes," *J. of Comp. Physics*, Vol. 43, 1981 pp. 357-372.
8. Hariharan, N., "High Order Simulation of Unsteady Compressible Flows Over Interacting Bodies with Overset Grids", *Doctoral Thesis*, School of Aerospace Engineering, Georgia Institute of Technology, Atlanta, GA 30332, August 1995.
9. Launder, B. E. and Spalding, D. B., "The Numerical Computation of Turbulent Flows," *Computational Methods in Applied Mechanics and Engineering*, Vol. 3, 1974, pp. 269-289.
10. Hao, Y., and Tao, Y.-X., "Melting of a Solid Sphere under Forced and Mixed Convection: Flow Characteristics," *Journal of Heat Transfer*, *ASME Trans.*, v 123, n 5, pp 937-950, 2001.

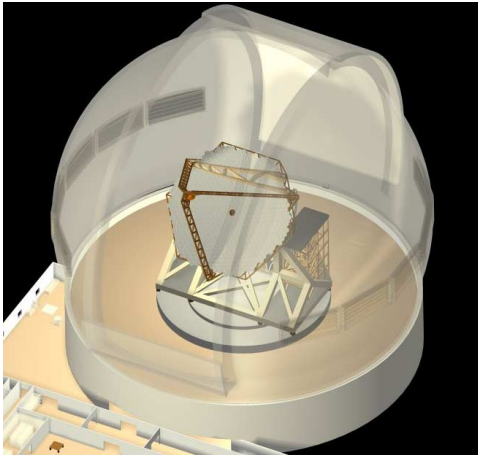


Figure 1 The Point-Design GSMT Structure
(Courtesy of AURA NIO)

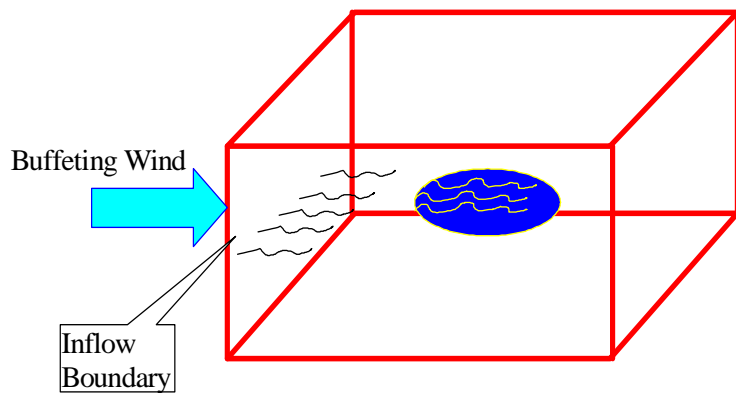


Figure 2 Physical Space Modeled Extends to 120 Meters
Upwind and Downwind

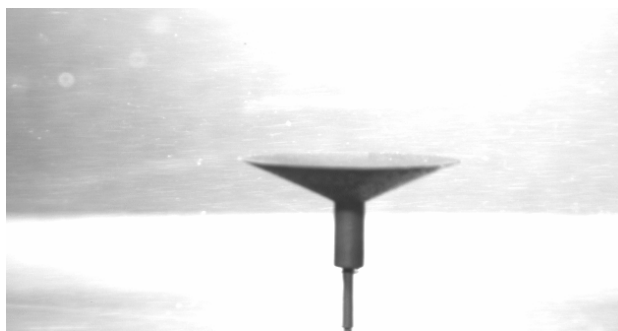


Figure 3. The Model of the Primary Mirror in the Water Tunnel

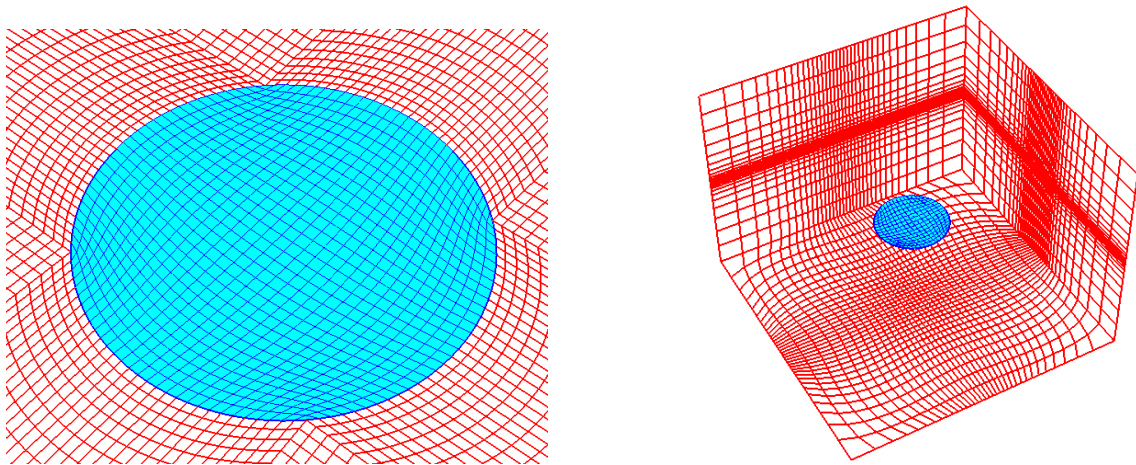
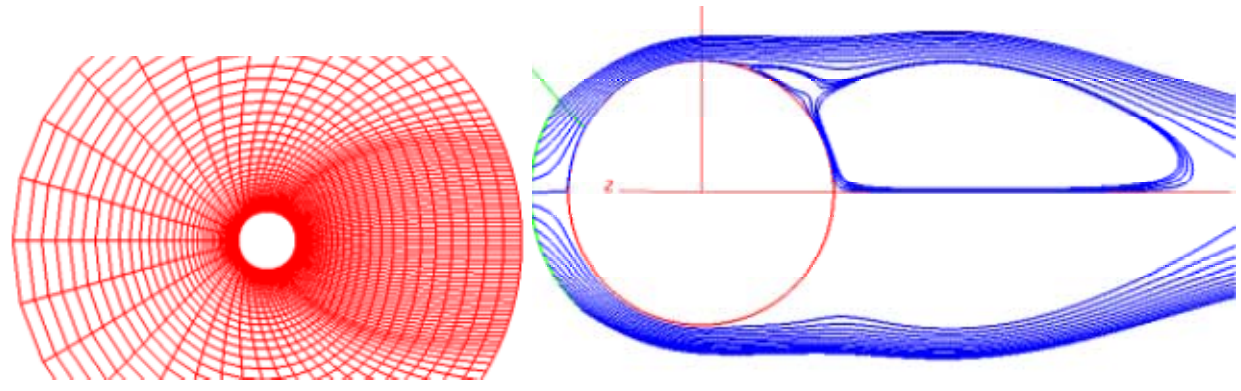


Figure 4. Local and Overall Body Fitted H-H Type Grid for 30 meter GSMT Primary Mirror



(a) O-H type grid for Cylinder (b) Traces of Fluid Particles Released Upstream of the Cylinder

Figure 5. Validation of the Solving Module Using Unit Circle (flow from left to right)

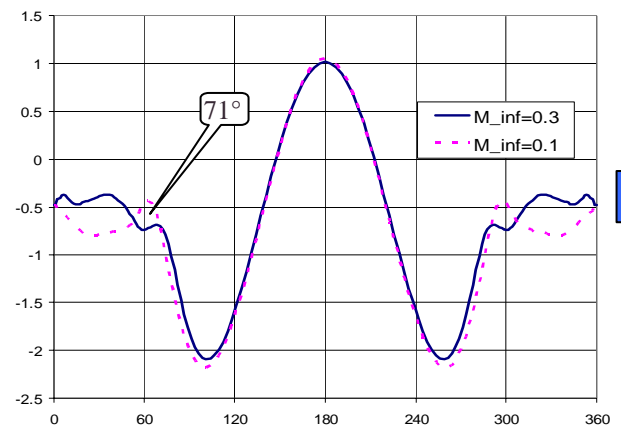


Figure 6. Effect of Numerical Mach Number for Circle

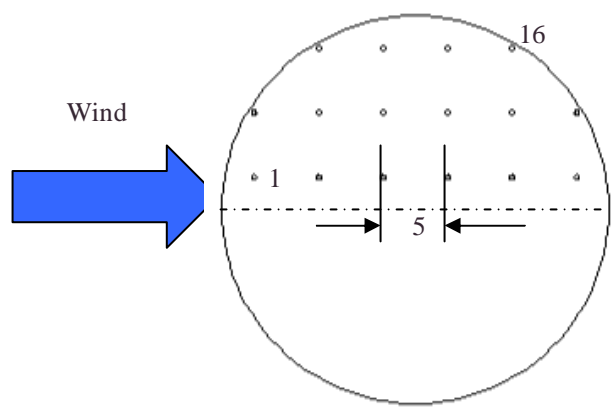
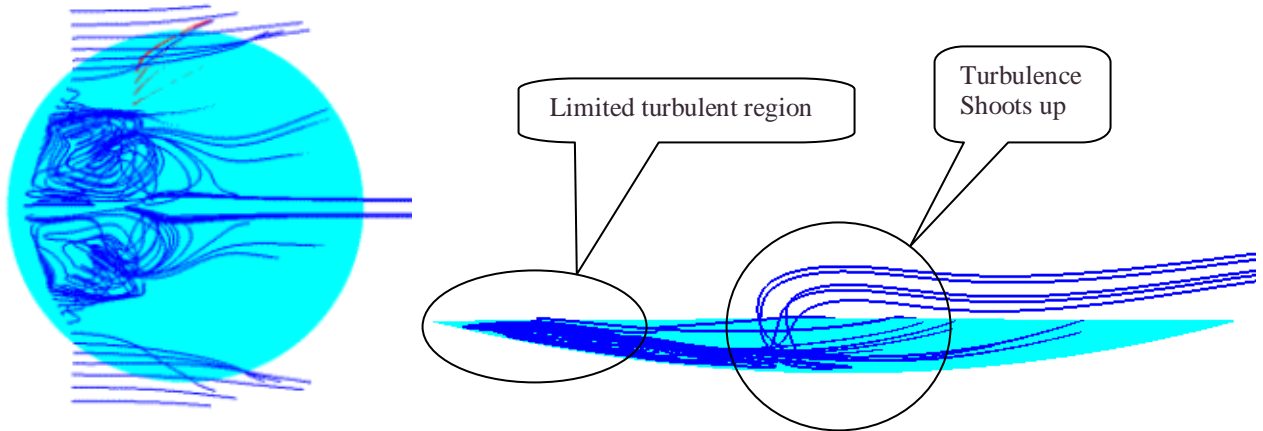


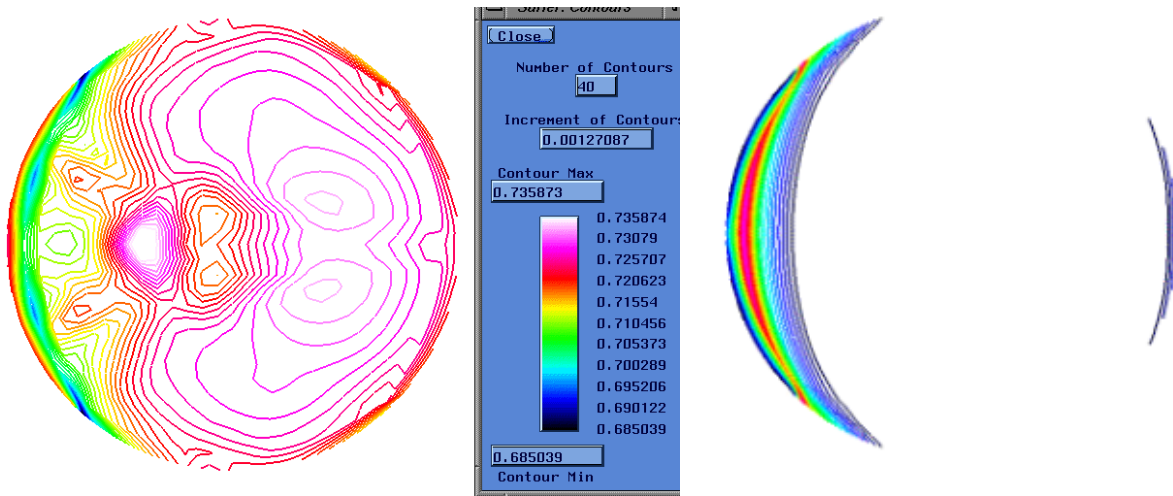
Figure 7. Relative Positions Where Dynamic Wind Loading is Calculated



8a. Top view

8b. Side view (cut from center plane)

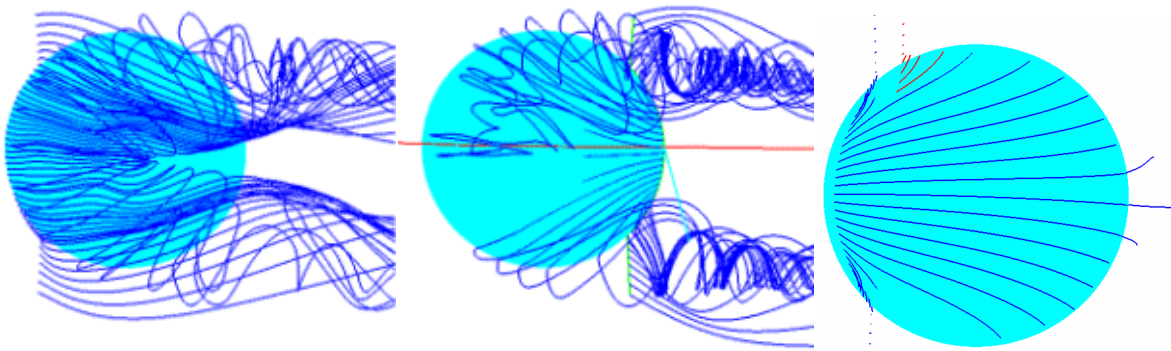
Figure 8. The Particle Traces for the 30m GSMT Mirror at 0° Impinging Angle in 8m/s Wind



9a. Upper Surface

9b. Lower Surface

Figure 9. The Pressure Contour the 30m GSMT Mirror at 0° Impinging Angle in 8m/s Wind

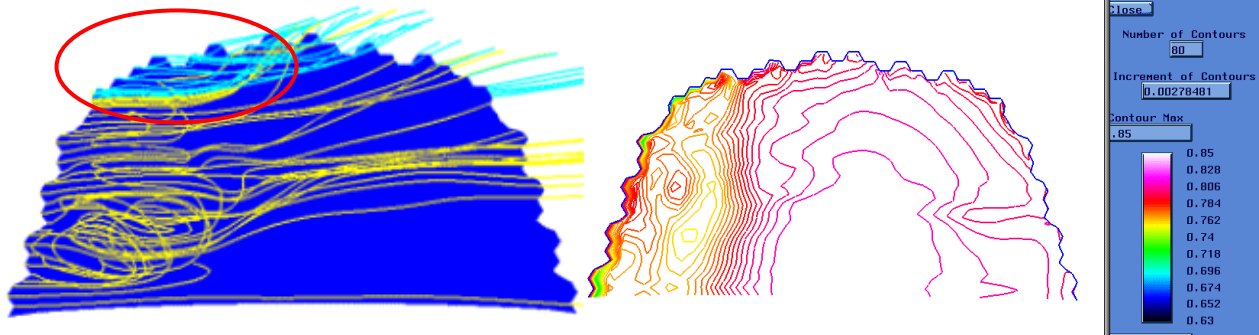


10a. Particles from leading edge

10b. Particles from trailing edge

10c. Upper Mirror Surface

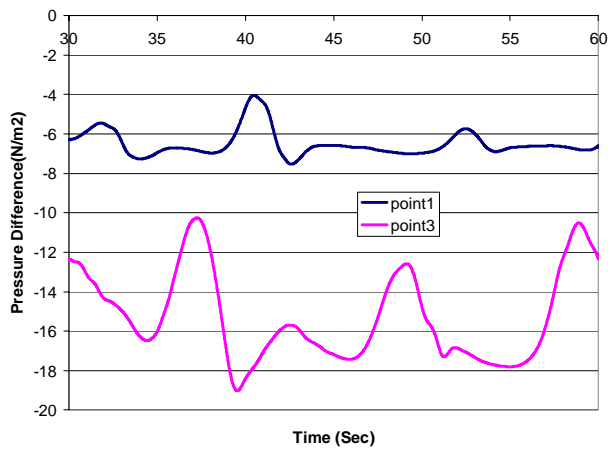
Figure 10. The Particle Traces for the 30m GSMT Mirror at 35° Impinging Angle in 8 m/s Wind
(10a and 10b show trace lines under the mirror, and 10c shows those above the mirror)



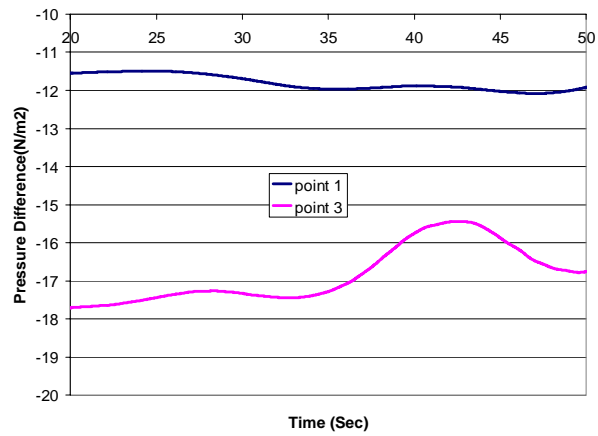
11a, Flow Field Traces.

11b. Pressure Contour

Figure 11. Flow Field and Pressure Map for GSMT Mirror with Serrated Edge at 0° impinging angle and 8 m/s Wind



12a. round mirror edge



12b. serrated mirror edge

Figure 12. The Unsteady Pressure Difference at Point No. 1 and Point 3

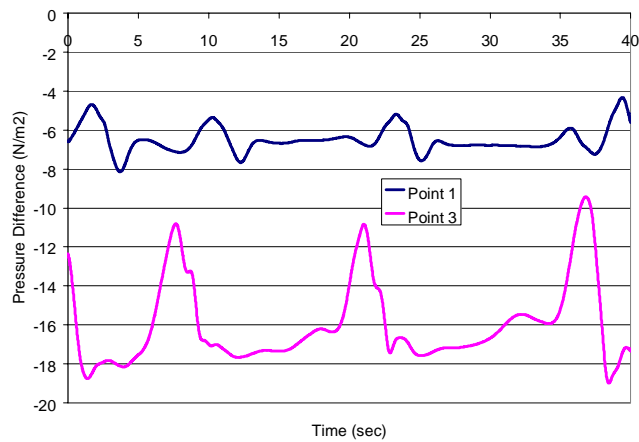


Figure 13. Calculated Dynamic Wind Loading at Point No. 1 and Point No. 3 for 2 m/s, 0.5 Hz Wind Buffeting on 8 m/s Mean Wind

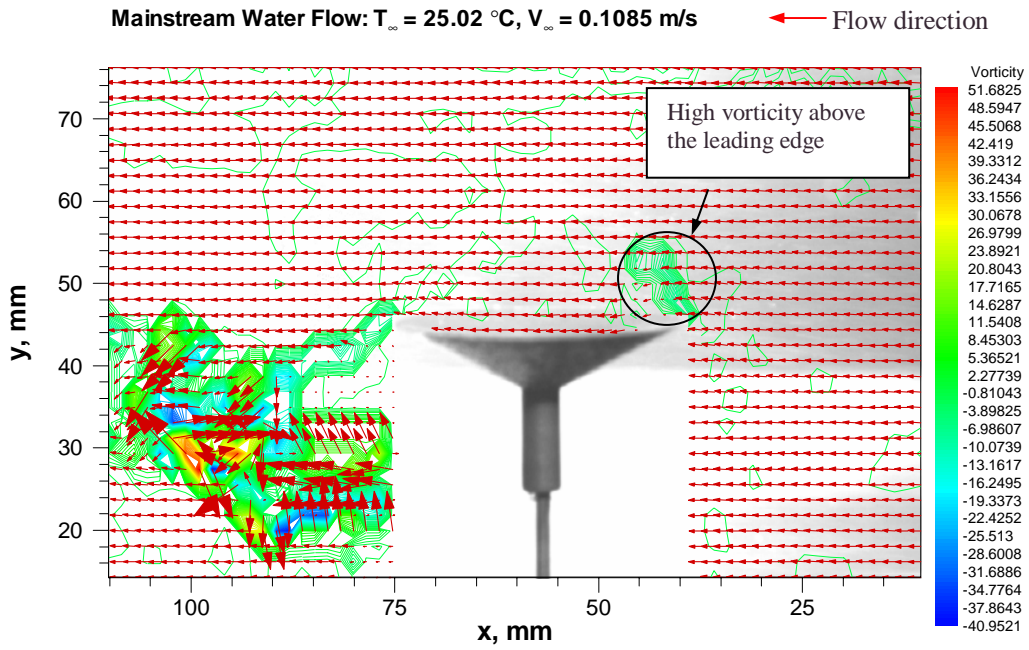


Figure 14. 9-degree Angle Side view of Flow Field on the Vertical Center Plane

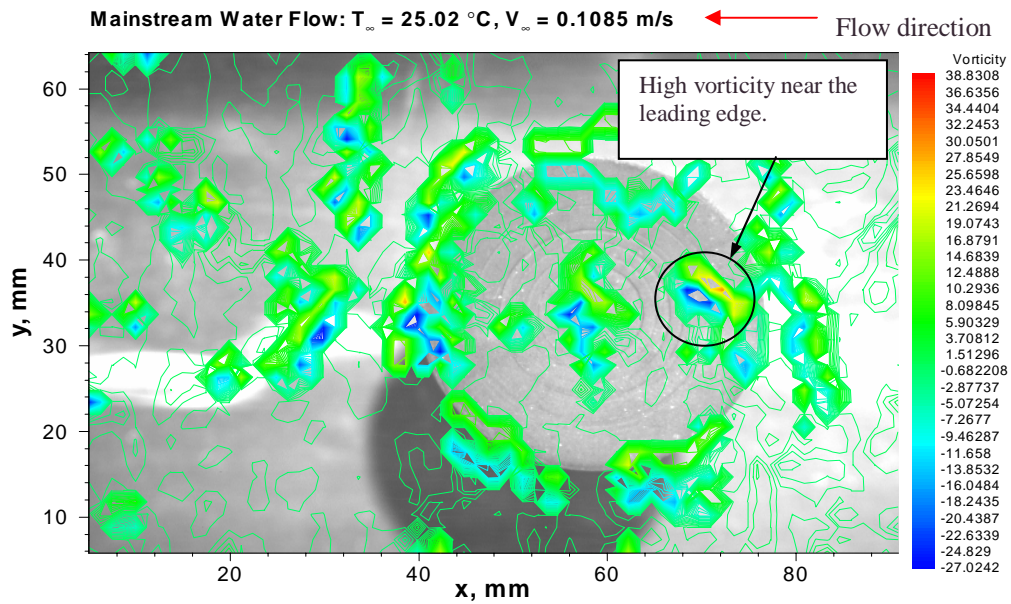


Figure 15. Top View of the Horizontal Plane about 2 mm Above the Mirror Edge Plane